Title

Vortex pinning by surface geometry in superfluid helium

Journal

Physical Review B, 89(10)

ISSN

2469-9950

Authors

Neumann, IH
Zieve, RJ

Publication Date

2014-03-01

DOI

10.1103/physrevb.89.104521

Peer reviewed

Vortex pinning by surface geometry in superfluid helium

I.H. Neumann and R.J. Zieve
Physics Department, University of California at Davis

We present measurements of how a single vortex line in superfluid helium interacts with a macroscopic bump on the chamber wall. At a general level our measurements confirm computational work on vortex pinning by a hemispherical bump, but not all the details agree. Rather than observing a unique pin location, we find that a given applied velocity field can support pinning at multiple sites along the bump, both near its apex and near its edge. We also find that pinning is less favorable than expected. A vortex can pass near or even traverse the bump itself with or without pinning, depending on its path of approach to the bump.

Vortex methods have appeared for decades in computational work on classical fluids in both two and three dimensions [1, 2]. They track the vorticity, which is the curl of the velocity field, rather than the velocity itself. The velocity can then be extracted using the Biot-Savart law. Vortex methods apply naturally to situations where the vorticity is concentrated in particular regions of the fluid; applications range from simulating trailing vortices of aircraft [1] to doing time updates of the computer graphics in video games [3]. A main benefit is that evaluating the velocity field does not require tracking a fine grid of points.

A complication for vortex methods is the treatment of the vortex cores, which in classical fluids change shape and size as vortex lines bend and move. Using a fixed size for the vortex cores, while more straightforward in conception and implementation, is valid only when the core size is small compared to all other length scales, including the local radius of curvature of the vortex and the spacing between the computational points along the vortex [4]. This restriction does apply naturally in superfluid ^{4}He, where the experimentally measured core radius is about 1.3Å, small enough to be ignored on typical computational and experimental length scales. Conveniently, direct comparison between superfluid hydrodynamics calculations and experiment becomes possible. In several cases such simulations accurately describe non-trivial experimental behaviors [5, 6].

Here we compare vortex pinning in experiment and calculation, finding discrepancies that may indicate a need to modify the computational treatment of surfaces. Our measurements track a single vortex in superfluid helium interacting with a macroscopic bump. We compare to the computational work of Schwarz [7], for a hemispherical bump on an otherwise flat wall. Schwarz uses a flow field that far from the bump is uniform and parallel to the wall. He finds that if the vortex is swept into the vicinity of the bump, the bump can capture and pin the vortex [7]. If the flow velocity is large the vortex continues to move, but for sufficiently low velocities it remains at the bump. The calculation uses no explicit pinning forces; rather, the stationary configuration comes about entirely from the vortex settling into an arrangement where the net velocity vanishes along its core. For a given flow velocity, the pinned vortex terminates at a unique position on the bump, in the plane perpendicular to the flow. As the velocity increases, the pin site moves out along the bump towards the wall.

Our experimental work confirms the general picture of a vortex pinning at a bump, but we find some key differences. First, we observe pinning near both the apex and the edge of a bump, for the same applied velocity field. Second, in Schwarz's work even a vortex on a path that avoids the bump can be pulled off course, encounter the bump, and pin to it. By contrast, we find that vortices only pin on the bump if they encounter it directly and sufficiently close to its center.

Our data come primarily from a cylindrical cell of diameter 5.79 mm, with a large bump midway along its length on the curved wall. At its widest point this bump has a roughly circular cross-section of diameter 3.05 mm, and its apex protrudes a distance 1.27 mm from the circular wall. As described elsewhere [6], the cell is mounted on a pumped ^{3}He cryostat and filled with ^{4}He through a small inlet hole in one end. Our measurements use a fine wire stretched vertically through the container, and a constant horizontal magnetic field of order 25 mT. The inset of Figure 1a depicts this geometry. We pass a brief current pulse through the wire; because of the static magnetic field, this creates a force displacing the wire from its equilibrium position. After the pulse ends, the wire's tension causes it to vibrate and ultimately to settle back to its equilibrium position. As the wire moves, we monitor the emf induced across it due to the horizontal magnetic field.

We create vortices by rotating the cryostat at low temperatures, but we make all our measurements with the cryostat stationary. Vorticity trapped around all or part of the wire alters the observed vibration frequencies. We focus on the frequency splitting between the two lowest modes. The earliest measurements with a straight vibrating wire [8] confirmed that circulation is quantized in superfluid helium, since the frequency splitting expected from a single quantum of circulation was strikingly stable. However, intermediate values of the frequency splitting also occur. These levels appear when a quantized vortex covers only a fraction of the wire and hence has a reduced effect on the vibration frequencies. From the observed signal we can identify the spot where the vortex leaves the wire. The vortex must then continue through the fluid as a free vortex, and that free portion moves at the local fluid velocity. Since this motion often leads to small adjustments to the position where the vortex leaves the wire, our vibrating wire measurements allow us to track the free vortex portion.

In our physical experiment, the driving field is the flow field of the trapped vertical vortex, which sweeps the free vortex segment around the cell. The free vortex terminates on the cell wall, and if it encounters the bump during its precession, it can pin to the bump. The resulting experimental signature is

that the circulation along the wire stabilizes; the steady energy loss that we observe during precession ceases, as does the oscillatory signal which corresponds to the circuit of the vortex around the wire.

As a first indication that there is more than one metastable configuration for the vortex on the bump, we observe not one but *three* closely spaced levels for stable circulation. Two appear in Figure 1. On approaching the bump, the vortex first pins with 20.7 mm of the wire's length covered by circulation. After several minutes, this level changes to 22.0 mm. Figure 2 includes the remaining level, at 19.6 mm. The differences between these heights are comparable to the widest radius of the bump. Thus the middle level may correspond to pinning at the apex of the bump, while the other two levels indicate pinning close to the top and bottom of the circle where the bump meets the wall.

Kelvin waves during the pins confirm that the three levels correspond to pinning at different parts of the bump. The Kelvin waves appear as rapid oscillations superimposed on the steady circulation. We have shown previously that Kelvin waves can be excited by our vibrating wire itself, particularly when the other end of the vortex is fixed [9]. From our earlier work, the observed oscillation frequencies correspond to the longest-wavelength modes with the vortex fixed at the cell wall and free to move vertically along the wire. (Empirically, since we observe oscillations at the Kelvin wave frequency, the vortex must not be fixed at the wire.) The wire used for the present measurements exhibits Kelvin waves often, and their frequencies provide key geometric information.

Frames b) and c) of Figure 1 expand the oscillations visible at each of the two stable circulation levels. The horizontal axis has the same scale in both cases, illustrating clearly that the oscillations at the first pin have a higher frequency. The periods are about 52 seconds for the first pinned level and 101 seconds for the second level. The period repeats to within the uncertainty of about two seconds for all pinning events at the same level.

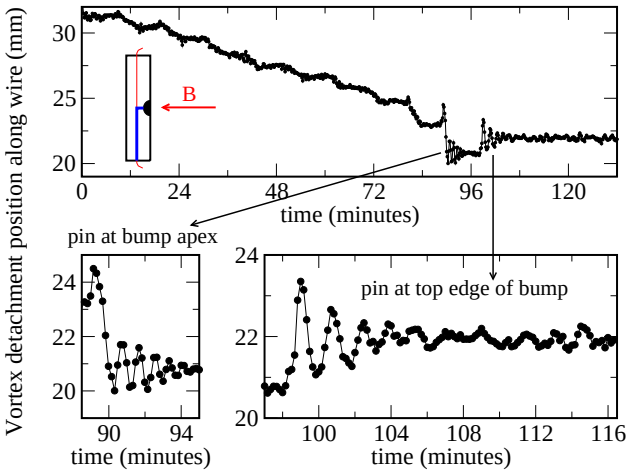

FIG. 1. Top frame, inset: cell geometry, with wire stretched near cell axis, a perpendicular magnetic field used to excite and detect the wire's vibration, and a bump on the side wall. As drawn a vortex extends along the wire from the bottom of the cell to the center, then leaves the wire and terminates on the bump. Top frame, main: motion of the end of the vortex along the wire. Initial oscillations correspond to the free vortex precessing through the cell. Pinning begins near 90 minutes. Lower frames: expanded views of the Kelvin waves that occur while the vortex is pinned. The two frames have the same horizontal scale.

The ideal Kelvin wave period in the long-wavelength limit is

$$T = \frac{2\lambda^2}{\kappa \ln \frac{\lambda}{2a_o}},$$

where $a_o = 1.3 \times 10^{-7}$ mm is the vortex core radius, $\kappa = 9.97 \times 10^{-2}$ mm^2/s is the circulation of the vortex, and λ is the wavelength of the Kelvin mode [10]. For a vortex with one end pinned, the lowest-frequency mode has wavelength four times the length of the free vortex segment. If the pin site is at the bump apex, then the free vortex length is 1.6 mm and the corresponding period is $T = 48$ seconds, very close to the observed value at the middle pin level. A pin site at the edge of the bump, with vortex length equal to the cell radius of 2.9 mm, gives a period of 164 seconds. Here the agreement is not especially good, although that could mean simply that the vortex does not pin precisely at the edge of the bump. Indeed, if we model the exposed half of the bump as half of an ellipsoid, then the straight-line path from the center of the cell to the bump edge passes *through* the bump. The observed period of 101 s suggests a vortex length of 2.3 mm. For our bump, this would occur at a distance 1.2 mm from the bump axis, which is still quite close to the edge laterally.

The Kelvin waves at the third pin level have an intermediate period near 62 seconds. This corresponds to a vortex length of 1.76 mm, which would place the pin site 0.97 mm off the

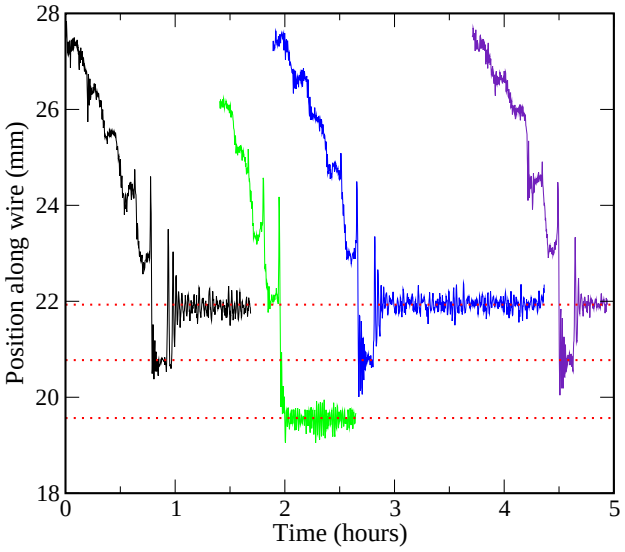

FIG. 2. Several approaches of a vortex to the bump, showing the reproducibility of the pin levels. Each curve has an arbitrary horizontal shift.

axis. Since the glue ran down in this direction when the bump was affixed to the cell wall, this edge does have a more gradual height change and the observed values for the pin location and Kelvin wave period are plausible.

Figure 2 is a compendium of several vortex pinning events. In three cases a vortex pins to the bump apex, then works free spontaneously after about 8 minutes and shifts to a site closer to the bump edge. By contrast, the pins at both the top and bottom edges of the bump never come free without deliberate heating on our part to dislodge the vortex. Thus it appears that for this geometry pinning to the bump apex is less stable than pinning closer to the bump edge. This temporary pinning does not occur in the computational work [7]. One possible reason for the difference is the much lower dissipation in our actual experiment. The computational vortices are far more able to dispose of excess length through Kelvin oscillations and the resulting energy loss; in our experiment, the oscillations may continue at high amplitude and eventually dislodge the vortex.

As noted above, both the pin levels and the Kelvin wave periods for each level are highly reproducible, strongly suggesting that vortices repeatedly pin at the same few spots. However, the initial approaches of the vortices are far from identical. Each trace begins with a few cycles of a slow oscillation, with period about 10 minutes. This feature corresponds to precession about the wire of the free vortex segment. Minima and maxima in this precession indicate particular directions of the free vortex within the cell. Since the heights of the minima and maxima vary from one trace to another, the different vortices must approach the bump along different trajectories but still reach the same pin locations. This cannot occur purely from microscopic roughness at the pin site; macroscopic energy considerations must play a role in guiding the vortex to the site. Similarly, the three vortices that move from a pin site at the bump apex to one at the bump edge trace out different paths. For example, as Figure 2 shows, the number of large-amplitude Kelvin wave periods before the vortex settles is different for each trace.

One unusual energy consideration that could contribute to the existence of multiple pin sites is the Gaussian curvature of the surface [11, 12]. Regions of negative Gaussian curvature are predicted to be more favorable for defects than regions of positive curvature. The arguments rely on energetics of two-dimensional systems, and a proposed test in superfluid helium involves a thin layer of superfluid [11]. In a three-dimensional system, surface energy terms are likely to be much smaller than bulk terms, but they may still provide an incremental contribution that leads to a metastable pin location.

A Gaussian curvature effect could explain the particularly unexpected location of one of our pin sites. Since the vortex must be perpendicular to the bump at its pin location, any pin site other than the bump apex requires the vortex to curve. For a stable pinned vortex, the velocity field produced by this curvature exactly cancels the applied velocity field. Following this logic, in our experiment we expect the stable pin site to lie towards the bottom edge of the bump. Yet our measurements repeatedly show a vortex pinning near the *top* edge, where the self-induced velocity near the bump augments the applied velocity. A pinning force, perhaps deriving from the energetics of Gaussian curvature, is needed to retain the vortex at this spot.

Another result from Schwarz's calculations is that if the fluid velocity is low enough for a vortex to pin, then the vortex will do so as long as it moves along a path that passes within about one bump radius of the edge of the bump [7]. The distortion of the velocity field by the bump pulls the vortex inward until it encounters the bump. By contrast, we find that whether or not the vortex pins depends strongly on its exact approach to the bump. The spikes in Figure 2 in the two or three precession cycles immediately before a vortex pins indicate that the vortex is moving over the surface of the bump but not pinning. If the end of the vortex traverses the bump, then the length of the free vortex shrinks abruptly. The length of circulation trapped on the wire increases sharply to compensate, causing the spike in our data. As the level at which the vortex encounters the bump approaches the bump center, the spike magnitude increases. For certain approach paths the vortex pins at the bump, although for others with essentially the same applied velocity field the vortex does not pin. The difference from the simulations may stem from our lower dissipation or from our applied velocity field's not being uniform.

A different geometry provides additional evidence that a vortex can pin at the edge or apex of a bump. In this cell the bump is attached not to the side wall but to one of the endcaps, with the wire glued to the bump apex. Thus a vortex that is trapped along the entire length of the wire terminates at the apex. Alternatively, a vortex that leaves the wire shortly before it reaches the bump and traverses the superfluid as a free vortex can pin near the edge of the bump. We cannot distinguish these two situations directly. In principle the beat frequency is slightly smaller if the vortex does not cover the entire wire. Unfortunately, for any reasonable configuration the missing length would be quite small, and the frequency difference would be unobservable. In part this is because the measurement sensitivity is vastly reduced near the ends of the

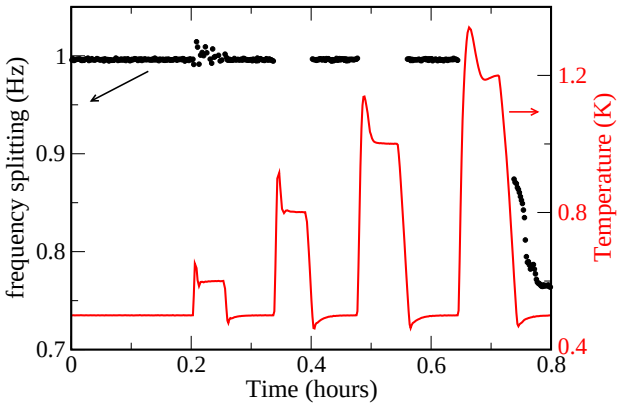

FIG. 3. Thermal cycling to depin a vortex from the wire; see text for details. Right (red) axis is temperature; left (black) axis is the frequency splitting of the lowest modes of the wire. The trace begins with a single quantum of circulation surrounding the entire wire; coincidentally, the frequency splitting for this circulation happens to be very close to 1 Hz.

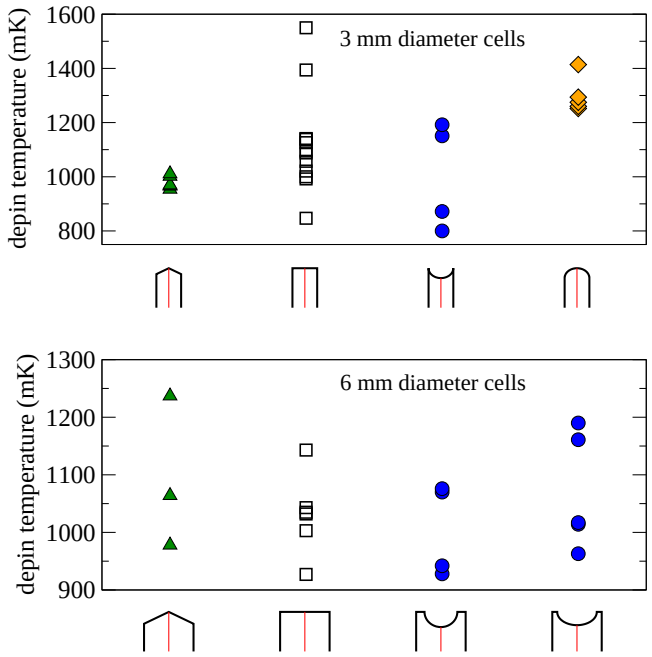

FIG. 4. Depin temperatures for eight cells. The shape of the cell's end cap (cone, flat, bump, or hemispherical indentation) is sketched below the data points for that cell. All caps have cylindrical symmetry. Each point corresponds to a single pinned vortex and indicates the temperature reached when the vortex left the wire. For the vortex shown in Figure 3, this temperature is 1.34 K, the maximum temperature of the final heating cycle.

wire compared to the middle. The wire's displacement during vibration has nodes at the ends of the cell, so circulation near the ends has little influence on the wire's motion.

However, we do observe an indirect signature related to the stability of pinned vortices. Figure 3 illustrates how we test stability. We provide thermal energy by raising the temperature of the cryostat. At the higher temperatures the damping of the vibrating wire is too high to extract the circulation, so after a few minutes we cool the cryostat and check whether the circulation level has changed. If it has not, we heat again to a slightly higher temperature, repeating until the vortex depins. After the vortex dislodges, the ensuing precession signal indicates that the vortex now lies along only part of the wire's length, with one end terminating on the cylindrical wall.

Figure 4 shows the temperatures at which vortices depin for several cells with different endcap configurations. Each point represents a single pinned vortex, with the temperature derived from a heating sequence such as that in Figure 3. Many of the cells show a large spread of depinning temperatures for different vortices, possibly depending on details of the heating cycles or on the interplay between the circulation and the end of the wire. Nonetheless, some patterns emerge, such as the high stability of vortices in the cell that ends with the hemispherical indentation. Three of the eight cells have endcaps with bumps. In those three, but not in any others, the depin temperatures cluster into two groupsm which may correspond to pinning at the bump apex and at the bump edge. A vortex pinned at the bump edge is already close to the outer wall of the cylinder, and we expect it to have a smaller energy barrier to overcome in depinning compared to a vortex that follows the entire wire. Hence the lower-temperature depins for each bump could occur for vortices pinning near the bump edge, while those at higher temperature signify vortices pinning at the apex. We note that the thin cell with a bump has some particularly low depin temperatures and also has the closest approach of the bump edge to the outer wall of the cell.

Our measurements agree with the qualitative picture of vortex pinning that arises from numerical simulations. However, given the past successes of superfluid hydrodynamics calculations, the discrepancies may indicate additional physics not accounted for in the computations. We observe multiple metastable pin sites on a single convex bump. In addition, vortices passing near the bump do not spiral inward and pin. On the contrary, even vortices that encounter the bump directly sometimes pass over it without pinning. We are pursuing further computational and experimental work to resolve these issues.

We acknowledge funding from UC Davis.

[1] A. Leonard, "Vortex methods for flow simulation," *J. Comput. Phys.* **37**, 289 (1980).
[2] A. Ojima and K. Kamemoto, "Vortex method simulation of 3D and unsteady vortices in a swirling flow apparatus experimented in 'Politechnica' University of Timisoara," *IOP Conf. Series: Earth and Environmental Science* **12**, 012065 (2010).
[3] A. Angelidis, F. Neyret, "Simulations of smoke based on vortex filament primitives," *Eurographics/ACM Siggraph Symposium on Computer Animation*, K. Anjyo and P. Faloutsos, ed. (2005).
[4] V.M. Fernandez, N.J. Zabusky, and V.M. Gryanik, "Vortex intensification and collapse of the Lissajous-elliptic ring: single- and multi-filament Biot-Savart simulations and visiometrics," *J. Fluid Mech.* **299**, 289 (1995).
[5] K.W. Schwarz, "Unwinding of a single quantized vortex from a wire," *Phys. Rev.* **B47**, 12030 (1993).
[6] L. Hough, L.A.K. Donev, and R.J. Zieve, "Smooth vortex precession in superfluid ^{4}He," *Phys. Rev. B* **65**, 024511 (2001).
[7] K.W. Schwarz, "Three-dimensional vortex dynamics in superfluid ^{4}He: Line-line and line-boundary interactions," *Phys. Rev. B* **31**, 5782 (1985).
[8] W.F. Vinen, "The detection of a single quantum of circulation in liquid helium II," *Proc. Roy. Soc. London A***260**, 218 (1961).
[9] R.J. Zieve, C.M. Frei, and D.L. Wolfson, "Energy loss from a moving vortex in superfluid helium," *Phys. Rev. B* **86**, 174504 (2012).
[10] R.J. Donnelly, *Quantized Vortices in Helium II* (Cambridge University Press, Cambridge, 1991).
[11] V. Vitelli and A.M. Turner, "Anomalous coupling between topological defects and curvature," *Phys. Rev. Lett.* **93**, 215301 (2004).

[12] V. Vitelli and D.R. Nelson, "Defect generation and deconfinement on corrugated topographies," *Phys. Rev. E* **70**, 051105 (2004).